Available online at www.ijpe-online.com

International Journal of Performability Engineering

vol. 15, no. 7, July 2019, pp. 1868-1877
DOI: 10.23940/ijpe.19.07.p13.18681877

Comparison of Fatigue Reliability Life of Telescopic Rod of an Eccentric Telescopic Rod Conveyor with and without Strength Degradation

Yingsheng Mou, Zhiping Zhai*, Xiaoyun Kang, Zhuwei Li, and Yuezheng Lan

College of Mechanical Engineering, Inner Mongolia University of Technology, Hohhot, 010051, China

Abstract

Eccentric telescopic rod conveyors are used to convey straw from chain conveyors to the feeding and compression mechanism of the 4FZ-2000A type self-propelled straw harvesting baler. As the main working component, the telescopic rod endures higher dynamic loads while conveying the straw. This will make the telescopic rod prone to fatigue fracture. Therefore, it is necessary to find a feasible model that can accurately estimate the fatigue reliability life of the telescopic rod. In order to ensure the safe working of the eccentric telescopic rod conveyer, a mechanical model of the main bearing parts of the telescopic rod is established, and virtual prototype technology is used to obtain the work load spectrum borne by the telescopic rod. Static analysis of the telescopic rod using the finite element method shows that the telescopic rod experiences multi-axial stress fatigue, and the critical section is determined. The *S-N* curve equation of the structure modified by the surface mass and stress gradient, critical plane approach, Miner's cumulative fatigue linear damage model, and Gaussian normal distribution model of fatigue life are used to estimate the fatigue life of the telescopic rod. In order to predict the fatigue life of the telescopic rod accurately, fatigue reliability lives are calculated with and without consideration of the strength degradation. The results show that: (1) the fatigue life prediction without considering the strength degradation is far different from practical experience; the results obtained after considering the strength degradation are more conservative and more consistent with the actual fatigue lives. The prediction results are more accurate. (2) When the strength degradation is considered, the modified Gerber correction method is more accurate than the Goodman correction method. The results of this study can provide a reference for the fatigue reliability analysis and optimization of eccentric telescopic rod conveyors.

Keywords: eccentric telescopic rod conveyor; telescopic rod; fatigue reliability life; strength degradation; Gaussian normal distribution

(Submitted on March 13, 2019; Revised on May 25, 2019; Accepted on June 25, 2019)

1. Introduction

The 4FZ-2000A self-propelled straw harvesting baler is a combined machine for harvesting crop straw, and it mainly consists of components such as a header, chain conveyor, eccentric telescopic rod conveyor, feeding mechanism, compression mechanism, and knotting device. The eccentric telescopic rod conveyor can convey straw from the chain conveyor to the feeding mechanism, preventing straw congestion and entanglement effectively. At present, the main problem in the working of the eccentric telescopic rod conveyor is the large dynamic load endured by the telescopic rod, which is the main working part, while conveying the straw. This will accelerate the fatigue of the telescopic rod and finally lead to fracture.

Several studies have been conducted on the application of eccentric telescopic rod conveyors in film mulching and caragana pickup [1-3], but few studies have focused on its application in conveying. There is no clear design theory or method stated in these, as they mainly refer to the design of the telescopic finger mechanism of spiral finger conveyors.

Research on fatigue reliability life and strength degradation has been presented as follows. D'Amore et al. [4] developed a two-parameter model based on strength degradation, and its predictive reliability was checked on a series of

* Corresponding author.
E-mail address: ngdzhzhp@imut.edu.cn

fatigue life and residual strength data available in literature. The modelling approach showed that the fatigue life and residual strength are related to the statistical distribution of static strength. Zhao et al. [5] studied the fatigue properties of basalt fiber reinforced epoxy polymer (BFRP) composites and revealed the degradation mechanism of BFRP composites under different cyclic loading stress levels through the tension–tension fatigue tests. The tensile fatigue loading tests demonstrated that the change in fatigue strength is closely related to the long-term run-out cycles. Ince [6] proposed a new fatigue damage model based on deformation strain energy and compared it with the Morrow and the SWT models to assess their prediction capabilities in accounting for the mean stress effect on fatigue life by using experimental tensile and compressive mean stress fatigue data for 120-90-02 ductile cast iron, 7075-T651 aluminum alloy, and Incoloy 901 superalloy. The proposed model was found to provide the best life predictions for the mean stress fatigue life data of all three materials under the tensile and compressive mean stresses. Hwang et al. [7] examined the effect of mean stress on fatigue damage gradient correction function and conducted fretting fatigue experiments to obtain the fatigue life data with R values ranging from −1.0 to 0.3. The results revealed that fretting fatigue life decreases with an increased stress ratio. Bang et al. [8] proposed a modification of the UniGrow model to predict total fatigue life with the presence of a short fatigue crack by incorporating short crack propagation into the UniGrow crack growth model. Su et al. [9], based on the failure transformation and multi-dimensional kernel density estimation methods, proposed two strategies for time-dependent probability fatigue analysis considering random load and intensity degradation. A filtering gear reducer was presented as an example to validate the effectiveness of the proposed methods. Fu et al. [10] studied the evaluation method of multi-axial fatigue damage of the deck and U-rib weld of the steel bridge decks. Gao et al. [11] derived a new probability model of residual strength based on the equivalence between loading times-fatigue life (LT-FL) and cyclic stress-residual strength (CS-RS) interference models. The validity of the model was verified by fatigue test data of unidirectional carbon/epoxy composites.

In this context, for fatigue reliability life prediction, this study determines the fatigue life of the telescopic rod on the basis of a fatigue reliability model with and without considering the strength degradation. It compares it with the actual design life to construct a more accurate prediction model. The results of this study can provide a reference for reliability analysis and optimization of eccentric telescopic rod conveyors and similar mechanical structures.

The rest of this article is organized as follows. Second 2 analyzes stress and provides a numerical calculation method on the stress distribution of an eccentric telescopic rod. Section 3 proposes the fatigue reliability theory model with and without strength degradation. The fatigue reliability lives of the telescopic rod with and without strength degradation are compared and analyzed in Section 4. Section 5 provides conclusions.

2. Stress Analysis of Eccentric Telescopic Rod

2.1. Working Principle of Eccentric Telescopic Rod Conveyor

An eccentric telescopic rod conveyor consists of an active sprocket, drum, telescopic rod shaft bracket, telescopic rod shaft, telescopic rod, guide sleeve, drum shaft, driven sprocket, and eccentric regulating handle, as shown in Figure 1.

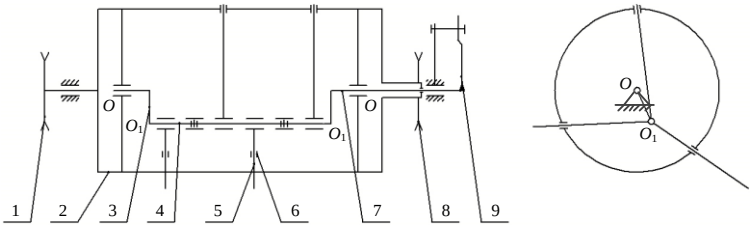

1. Active sprocket; 2. Drum; 3. Telescopic rod shaft bracket; 4. Telescopic rod shaft;
5. Telescopic rod; 6. Guide sleeve; 7. Drum shaft; 8. Driven sprocket; 9. Eccentric regulating handle.
Figure 1. Schematic diagram of eccentric telescopic rod conveyor

When working, the power source drives the active sprocket, which in turn drives the drum to rotate around the drum shaft/OO. Through the guide sleeve fixed on the drum, the telescopic rod rotates around the telescopic rod shaft/O_1O_1. The eccentric distance between the telescopic rod axis and drum axis is e, and the deflection angle of the telescopic rod axis can be adjusted by adjusting the position of the eccentric handle. When conveying materials, the extended length of the telescopic rod relative to the drum will gradually increase. After the conveying is completed, the telescopic rod will gradually reduce in length to prevent materials from returning. As can be deduced from its working, the eccentric telescopic rod mechanism is essentially a rotating guide-bar mechanism.

2.2. Mechanical Model of Eccentric Telescopic Rod

The following assumptions are made when establishing the mechanical model of an eccentric telescopic rod: 1) when the telescopic rod rotates around the telescopic rod shaft, the friction torque and friction of the telescopic rod that slides along the guide sleeve are negligible; 2) during operation, the end of the telescopic rod is loaded to the maximum, and hence the influence of material thickness is not considered; 3) the drum rotates at a constant speed irrespective of the thickness of the drum wall.

Figure 2 is the dynamic analysis diagram of an eccentric telescopic rod conveyor. Take O_1 as the origin of coordinates; the *X*-axis coincides with the telescopic rod, and the *Y*-axis is perpendicular to the telescopic rod to establish a plane rectangular coordinate system. O_1 is the hinge point between the telescopic rod and the telescopic rod axis. *A* is the intersection point between the guide sleeve and the axis of the telescopic rod. The telescopic rod O_1B is driven by the guide sleeve fixed on the drum. The telescopic rod is the main working part of the eccentric telescopic rod conveyor. The force acting on the telescopic rod is the driving force F_d of the guide sleeve supplied to the telescopic rod, and F_r is the resistance of the material at the end of the telescopic rod (concentrated at point B), which can be decomposed into the force F_x, the vertical force F_y, and the supporting reaction F_{R1} of the telescopic rod at the fulcrum O_1, which is set at an angle θ to O_1B.

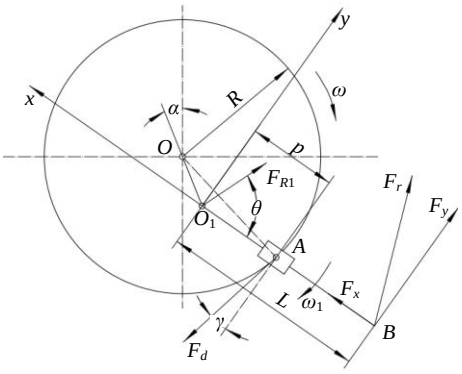

Figure 2. Dynamics analysis diagram of conveyor

When the eccentric telescopic rod conveyor works, the drum rotates at a constant speed, and the following mechanical model can be established:

$$\sum X = 0, \quad F_x + F_d \sin\gamma - F_{R1}\cos\theta = 0 \tag{1}$$

$$\sum Y = 0, \quad F_y - F_d \cos\gamma + F_{R1}\sin\theta = 0 \tag{2}$$

$$\sum M_{O_1} = 0, \quad F_y L - pF_d \cos\gamma = 0 \tag{3}$$

In conjunction with Equations (1) to (3):

$$F_y[(L-p)\cot\theta - L\tan\gamma] = pF_x \tag{4}$$

Where *L* is the length of the telescopic rod, *p* is the length of the telescopic rod in the drum, and γ is the angle between the traction speed and absolute speed of the telescopic rod in *A*. During transportation, F_x and F_y, the forces exerted by the materials on the telescopic rod, change with the rotation of the drum, and their specific values are related to the material characteristics, conveying capacity, working resistance, and motion parameters [12]. That is:

$$F_y = KQa_B[1+\tan^2(45°+\varphi)] \tag{5}$$

Where *K* is the correction coefficient of the conveying capacity, which is taken as 0.5 when conveying wheat straw; a_B is the instantaneous acceleration of point *B* at the end of the telescopic rod [13]; φ is the friction angle of the material and the telescopic rod, whose value ranges from 0 to 40.5 °for wheat straw; and *Q* is the conveying capacity in a cycle [13].

$$F_x = b(L-p)S\psi \sec^2(45°+\varphi) \tag{6}$$

Where b is the distance between two adjacent rods; ψ is the viscoelastic coefficient of the material, which is 2.2 for wheat straw; and S is the area over which the track at the end of the telescopic boom touches the material [13].

From Equations (5) and (6), the resistance of the material to the end of the telescopic rod F_r can be calculated:

$$F_r = \sec^2(45°+\varphi)\sqrt{K^2Q^2a_B{}^2 + b^2(L-p)^2S^2\psi^2} \tag{7}$$

Substituting Equations (5) and (6) into Equation (4) can determine θ:

$$\theta = arc\cot\left(\frac{pbS\psi}{KQa_B} + \frac{L\tan\gamma}{L-p}\right) \tag{8}$$

Substituting Equation (8) into Equations (1) and (2), the supporting reaction F_{R1} can be obtained as follows:

$$F_{R1} = \frac{F_x + F_d\sin\gamma}{pF_x + LF_y\tan\gamma} \times \sqrt{F_y^2(L-p)^2 + (pF_x + LF_y\tan\gamma)^2} \tag{9}$$

2.3. Acquisition of Telescopic Rod Load Spectrum

In order to obtain the load spectrum of the telescopic rod, firstly, the 3D model of each component of the conveyor is constructed using SolidWorks, and virtual assembly is performed. Secondly, it is imported into the virtual prototyping software ADAMS. After specifying the motion pair and drive, motion simulation is performed on the eccentric telescopic rod conveyor. Figure 3 shows the virtual prototype model built in ADAMS.

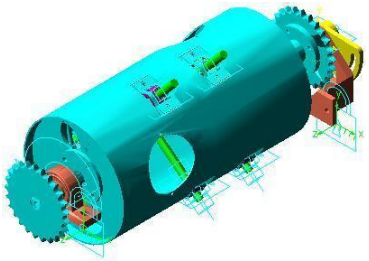

Figure 3. Virtual prototype model of the conveyor

Kinetic analysis of the conveyor shows that the telescopic rod is affected by the driving force F_d of the drum, material resistance F_r, and reaction force F_{R1}. In ADAMS, a rotary pair (drum-support) is selected to apply the actual drum operating speed of 265r/min, and the material resistance is applied to the end of the telescopic rod. In actual practice, the driving force F_d acts on the telescopic rod through the guiding sleeve on the drum; hence, one of the moving pairs (the telescopic rod-guide sleeve) is selected for the force measurement. One of the dot-line pairs (the telescopic rod-eccentric shaft) is selected, and the reaction force F_{R1} is measured. The load spectrum of F_r and F_d can be obtained as shown in Figure 4.

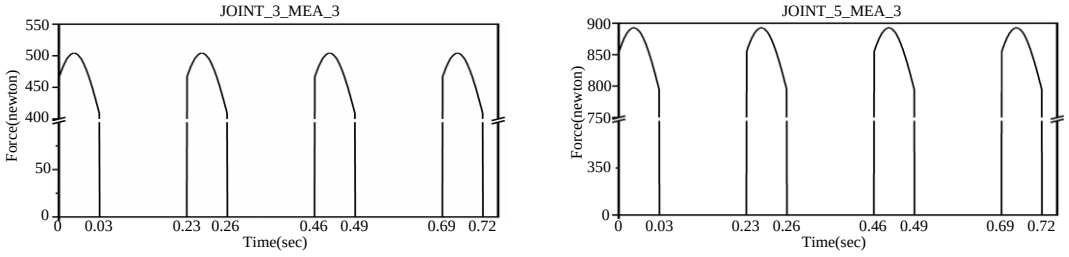

(a) F_r curve (b) F_d curve

Figure 4. Load spectrum of telescopic rod

2.4. Finite Element Static Solution and Load Mapping

In order to study the stress fatigue, the maximum load is assumed to be exerted on the established finite element model to obtain the stress on each unit node by using the finite element analysis software ANSYS Workbench. From this analysis, the equivalent stress distribution cloud map and the first, second, and third principal stress cloud maps (figure omitted) are obtained. From the equivalent stress distribution cloud map, it can be seen that the largest stress of 116.7MPa occurs at the joint between the telescopic rod and the guide sleeve. The maximum stress is much smaller than the yield strength of the material, and the fatigue of the telescopic rod can be classified as high cycle fatigue (stress fatigue). It can be seen from the first, second, and third principal stress cloud diagrams that the maximum values of the three principal stresses reduce sequentially and are all non-zero, so the fatigue of the telescopic rod can be classified as multiaxial.

For the static analysis, a unit load (1N) is applied to the telescopic rod, and the resulting stress data of each unit node is submitted for load mapping. The load mapping transforms the static solution from the finite element analysis of the telescopic rod into an alternating solution associated with the load spectrum. Considering the difficulty of obtaining load data of the telescopic rod during actual working, simulation is used to obtain the load spectrum, and the time series load obtained by the simulation described in Section 1.3 is used as the load spectrum of the telescopic rod.

Through the load spectrum, the stress under unit load of the telescopic rod can be transformed into the stress tensor history under actual working conditions. The stress tensor of the unit node X of a telescopic rod under two load spectra is:

$$\sigma_X(t) = \sigma_{1X} \times L_1(t) + \sigma_{2X} \times L_2(t) \tag{10}$$

Where $L_1(t)$ and $L_2(t)$ are two load spectra of the telescopic rod, and σ_{1X} and σ_{2X} are the stresses at point A when the unit load is applied in the two load directions.

2.5. Stress Combination

In general, a stress tensor has nine stress components. Considering the symmetry, this can be reduced to six. In order to perform equivalent conversion with the *S-N* curve stress data, an objective evaluation quantity, namely the principal stress, must be found. The principal stress is divided into the first, second, and third principal stresses.

This study uses the critical plane (critical surface) stress combination method, which can indicate the direction of damage and is used widely in engineering analysis. This method involves projecting the stress onto a critical surface and calculating the combined stress on multiple planes by the rain flow counting method.

As shown in Figure 5, the stress tensor is projected on the XY plane, and the stress is obtained by computing the stress at any given angle along the polar coordinates of the XY plane. The stress calculation formula for each plane is:

$$\sigma_\Phi = \frac{\sigma_{xx} + \sigma_{yy}}{2} + \frac{\sigma_{xx} - \sigma_{yy}}{2} \cos 2\Phi + \sigma_{xy} \sin 2\Phi \tag{11}$$

Where σ_{xx} is the principal stress along the X-axis, σ_{yy} is the principal stress along the Y-axis, and σ_{xy} is the shear stress in the XY plane.

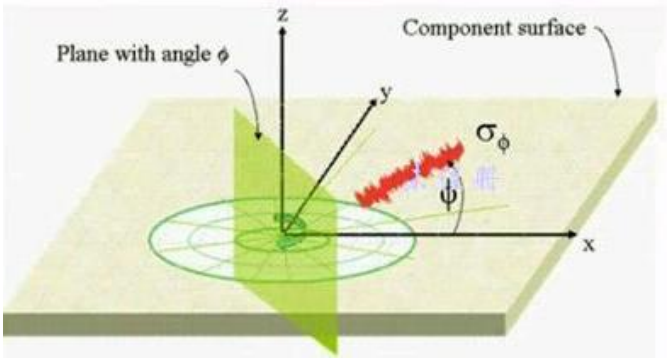

Figure 5. Dangerous combination

3. Fatigue Reliability Life Prediction

3.1. S-N Curve

Fatigue occurring in the telescopic rod can be classified as stress fatigue, and the damage calculation must be based on the *S-N* curve data of the material. The telescopic rod is fabricated using national standard 45 steel, which has a performance analogous to that of the American standard carbon steel SAE1045_shaft. The *S-N* curve is plotted for a symmetrical cyclic load on the test piece. The surface roughness of the telescopic rod is 6.3 μm, which is rougher than the test piece and easier to crack, necessitating the incorporation of surface correction in the *S-N* curve of the material [14]. It can be seen from Figures 8 and 9 that the joint between the telescopic rod and guide sleeve and the joint between the telescopic rod and rod shaft have stress concentrations, which result in a reduction of the fatigue strength of the telescopic rod, requiring a stress gradient correction.

After surface correction and stress gradient correction, the *S-N* curve is shown in Figure 6:

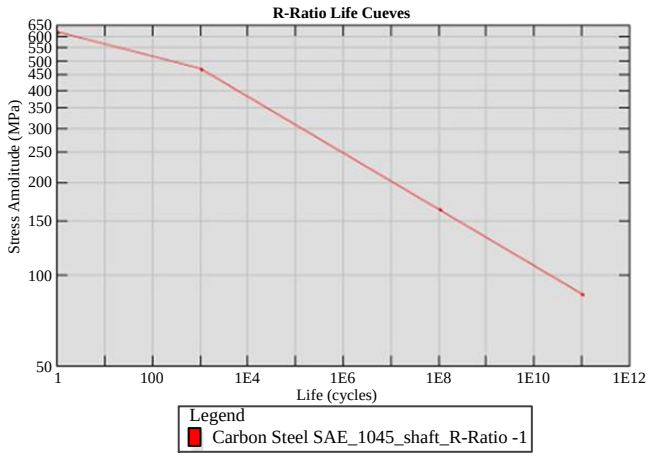

Figure 6. *S-N* curves of the telescopic rod

3.2. Average Stress Correction

The *S-N* curve of the standard specimen made of Carbon Steel SAE1045_shaft is measured when the average stress is zero. According to the load spectrum, the average stress of the telescopic rod is not zero, therefore, average stress correction of the telescopic rod is required. The actual stress state is converted to the symmetrical cyclic stress state of the test bar based on an equal life. This study uses Goodman's modified method and the improved Gerber correction method [6-7] for this purpose. The mathematical models are:

$$\frac{S_a}{S_{\max}} + \frac{S_m}{S_b} = 1 \tag{12}$$

$$\frac{S_a}{S_{\max}} - \left(\frac{S_m}{S_b}\right)^2 = 1 \tag{13}$$

Where S_a is the stress amplitude of components under actual working conditions, S_m is the average stress of components under actual working conditions, S_b is the tensile strength limit of material, and $S_{\max}$ is the maximum stress at a stress ratio of -1.

The Goodman and improved Gerber correction curves are shown in Figure 7. The Goodman correction curve is a straight line. When the average stress is greater than zero, the stress amplitude is smaller. When the average stress is less than zero, the stress amplitude is larger; this method is conservative. The improved Gerber correction curve is an improvement on the Gerber curve, and it involves adjusting the stress amplitude in the negative interval of the average stress. The improved Gerber correction curve can accurately predict the effect of the average tensile and compressive stress on fatigue, and it is more popular for engineering applications. Therefore, Goodman's and the improved Gerber modified

method are respectively used in this paper to modify the average stress of the eccentric telescopic rod.

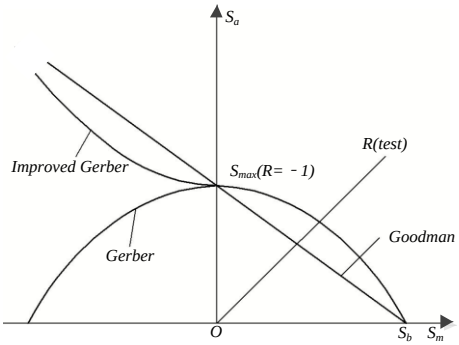

Figure 7. Mean stress correction curve

3.3. Fatigue Reliability Model Without Considering Strength Degradation

The reliability of fatigue data is also referred to as the survival rate. The unevenness of the material of the telescopic rod, difference in processing quality and size, test load error, and other factors lead to large discreteness in the fatigue data. Therefore, the method of statistical analysis is introduced to process fatigue data to obtain a clearer understanding of the fatigue performance. The *S-N* curve of the telescopic rod material is drawn at a survival rate of 50%, and its fatigue life follows a Gaussian normal distribution [15]. Its probability density function is:

$$f(x)=\frac{1}{\sigma\sqrt{2\pi}}e^{-\frac{(x-\mu)^2}{2\sigma^2}} \tag{14}$$

Other survival rates are obtained based on the normal distribution transformation, i.e.:

$$f(u)=\frac{1}{\sqrt{2\pi}}e^{-(\frac{1}{2}u^2)}, \quad u=\frac{x-\mu}{\sigma} \tag{15}$$

Where u is a standard normal distribution variable related to the survival rate, and it can be found from Table 1; μ is the logarithmic lifetime of the telescopic rod at 50% survival rate; σ is the variance of the material parameters and is set equal to 0.1; and x is the logarithmic lifetime of the telescoping rod at a given survival rate.

Table 1. Standard normal distribution variable and survival rate

Standard normal distribution variable (u)	Survival rate (%)	Standard normal distribution variable (u)	Survival rate (%)
3.0	0.1	-0.5	69.0
2.5	0.6	-1.0	84.0
2.0	2.3	-1.5	93.0
1.5	6.7	-2.0	97.7
1.0	16.0	-2.5	99.4
0.5	31.0	-3.0	99.9
0	50.0		

3.4. Fatigue Reliability Model Considering Strength Degradation

3.4.1. Residual Strength Degradation Model based on Fatigue Damage

Under a cyclic load, the accumulated damage inside the material of the mechanical component is continuously increased, resulting in the continuous degradation of its performance and reduction of the remaining life. The residual strength is the ability of the structure to withstand external loads after a period of service, and it is closely related to the loading method and frequency of loading. The residual strength of metals decay and degenerate slowly at first, and then they decrease sharply until fatigue damage occurs when the loading cycle ratio is closer to 1 than β [16]. In the previous analysis, the load applied to the telescopic rod has a constant amplitude. Schaff et al. stated that under the action of a constant amplitude load,

the residual strength $\delta(n)$ would degenerate exponentially [17]:

$$\delta(n) = \delta(0) - \left[\delta(0) - S_{\max}\right]\left(\frac{n}{N_f}\right)^c \tag{16}$$

Where n is the number of load actions; N_f is the fatigue life corresponding to the load; $\delta(0)$ is the static tensile strength σ_b, where σ_b of Carbon Steel SAE1045_shaft is 833.6MPa; $S_{\max}$ is the maximum value of the alternating load, which is 116.7MPa for the telescopic rod; c is determined by the residual strength degradation test data; and the c of the Carbon Steel SAE 1045_shaft material is 4.108 [15].

3.4.2. Distribution of Residual Strength and Fatigue Reliability Model Considering Strength Degradation

It can be seen from the previous analysis that the static strength of the telescopic rod material obeys the Gaussian normal distribution when the strength degradation is not considered, namely:

$$f\left(\delta(0)\right) = \frac{1}{\sigma\sqrt{2\pi}}\exp\left\{-\frac{\left(\delta(0)-\mu\right)^2}{2\sigma^2}\right\} \tag{17}$$

Therefore, the probability density function of residual strength is:

$$f(\delta(n)) = \frac{1}{\sigma\sqrt{2\pi}}\exp\left\{-\frac{(\frac{\delta(n)-S_{\max}\beta^c}{1-\beta^c}-\mu)^2}{2\sigma^2}\right\} \tag{18}$$

Where β is the loading cycle ratio, which is the ratio of the loading frequency n to the fatigue life N_f. It can be seen that when the initial strength $\delta(0)$ obeys the Gaussian normal distribution, the residual strength also conforms to the Gaussian normal distribution in the process of strength decay degradation.

Considering factors such as the dispersion of material properties and the instability of the technological process, the initial strength of the telescopic rod under a constant amplitude load is also a random variable. If the probability density of the initial strength of the telescopic rod is $f(\delta)$, when the load cycles n times considering the strength degradation, the reliability of the rod is [16]:

$$R(n) = \int_{-\infty}^{\infty} f(\delta)\prod_{i=1}^{n} F_s(\delta, i-1)\mathrm{d}\delta \tag{19}$$

4. Comparative Analysis of Fatigue Reliability Life of Telescopic Rod with and without Strength Degradation

The fatigue analysis module nCode SN TimeSeries of the nCode DesignLife software is selected, and the finite element results and load spectrum are imported into Simulation_Input and TSInput, respectively. The material property settings, *S-N* curve equation correction, and fatigue solution are performed in the fatigue analysis module StressLife_Analysis. Based on the linear Miner damage rule, the fatigue reliability life of the telescopic rod is calculated when the survival rate of the telescopic rod is 50%, 90%, and 99%, respectively; at the same time, the fatigue life of the telescopic rod is corrected by the Goodman and improved Gerber average stress. The cloud diagram of the obtained life without considering strength degradation is shown in Figures 8 and 9. The fatigue life prediction results can be obtained after finishing, as shown in Table 2.

It can be seen from Figures 8 and 9 and Table 2 that the minimum fatigue life of the telescopic rod with the same average stress correction method and the position of the critical point is different under different survival rates, the position of the danger point is also different, and the minimum fatigue life decreases with an increase in the survival rate. In addition, under the same survival rate, the fatigue life of the telescopic rod differs with different average stress correction methods. Moreover, the predicted fatigue life by the improved Gerber curve correction method is lower than that predicted by the

Goodman curve correction method, indicating that the improved Gerber curve correction method is more conservative.

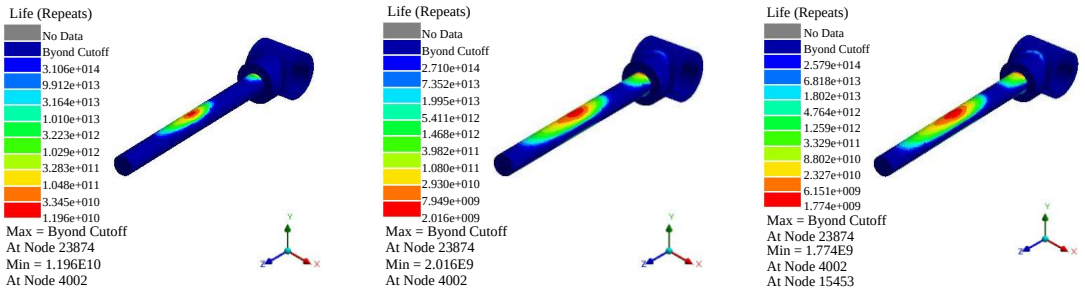

(a) Survival rate 50% (b) Survival rate 90% (c) Survival rate 99%

Figure 8. Fatigue life cloud map corrected by Goodman curve

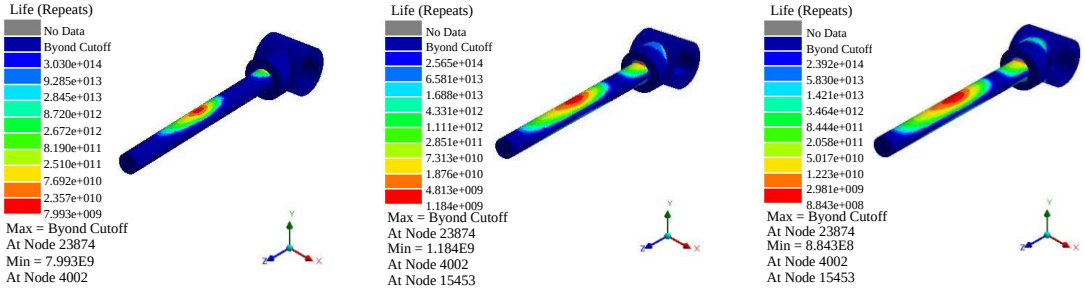

(a) Survival rate 50% (b) Survival rate 90% (c) Survival rate 99%

Figure 9. Fatigue life cloud map modified with improved Gerber curve

Table 2. Fatigue life comparisons with and without considering strength degradation (times)

Average stress correction method	Survival rate (%)	Fatigue life without considering strength degradation	Fatigue life considering strength degradation
Goodman	50	1.196e+10	2.392e+9
Goodman	90	2.016e+9	1.217e+9
Goodman	99	1.774e+9	1.014e+9
Improved Gerber	50	7.993e+9	1.599e+9
Improved Gerber	90	1.184e+9	5.974e+8
Improved Gerber	99	8.843e+8	5.053e+8

For ease of comparison, the fatigue life of the telescopic rod considering the strength degradation can be calculated using Equations (16), (18), and (19) on the basis of the computed fatigue life that did not consider the strength degradation, with 50%, 90%, and 99% survival rates and using the Goodman and improved Gerber average stress modified method, as shown in Table 2. It can be seen that the fatigue life of the telescopic rod is more conservative after considering strength degradation with the same mean stress correction method and same survival rate.

According to the national standard GB/T 34390-2017 for self-propelled straw harvesting baler, the working life of the eccentric telescopic rod conveyor at the survival rate of 90% is generally about eight years. Assuming that the conveyors work 300 days a year and ten hours per day, the working life of the telescopic rod is 15.514 years when the survival rate is 90% without considering strength degradation, and it is modified by the improved Gerber curve. Under the same condition but considering the strength degradation, the working life of the telescopic rod is 7.827 years. It can be seen that there is a remarkable gap between considering and not considering the strength degradation in the fatigue life computation. The fatigue reliability life of the telescopic rod is more in line with the actual life when the strength degradation is considered, and the prediction result is more accurate. When considering the intensity degradation, the improved Gerber correction method is more accurate than the Goodman correction method.

5. Conclusions

First, a mechanical model of the main bearing parts of the telescopic rod was established by analyzing the working principle and structural characteristics of the eccentric telescopic rod conveyor. Subsequently, the load spectrum of the telescopic rod was obtained by using virtual prototype technology.

Second, the *S-N* curve of the telescopic rod was obtained by surface quality and stress gradient correction. The CriticalPlane dangerous surface stress combination method and the linear Miner damage rule were used to calculate the fatigue reliability lives of the Goodman and improved Gerber curve correction models when the survival rate was 50%, 90%, and 99%, respectively. The calculation results showed that the improved Gerber curve correction method computes a lower fatigue life than the Goodman curve correction method, and the result is thus more conservative.

Finally, comparison of fatigue reliability life of the telescopic rod with and without strength degradation showed that there is a remarkable gap between the two computed values of fatigue life. The fatigue reliability life of the telescopic rod was more in line with the actual life when the strength degradation was considered, and the prediction result was more accurate. When considering the degradation in intensity, the improved Gerber correction method is more accurate than the Goodman correction method.

Acknowledgements

This work is supported by the Inner Mongolia Natural Science Foundation (No. 2018MS05059).

References

1. J. F. An, Y. Wang, T. Zhang, T. G. Wang, and F. W. Zhang, "The Improvement Design on Telescopic Rod Type Collecting Roller of Residual Film Recycling Machine," *Agricultral Equipment & Vehicle Engineering*, Vol. 52, No. 3, pp. 7-9, 2014
2. G. H. Li, Z. Zheng, Y. Zhao, and Q. Niu, "The Design and Improvement of Eccentric Roller Type Residual Film Pickup Device," *Xinjiang Farm Research of Science and Technology*, Vol. 38, No. 11, pp. 31-32, 2015
3. Z. Q. Tian, "Research on the Design of Caragana Picking and Shredder," Master Dissertation, Shanxi Agricultural University, 2014
4. A. D'Amore and L. Grassia, "Constitutive Law Describing the Strength Degradation Kinetics of Fibre-Reinforced Composites Subjected to Constant Amplitude Cyclic Loading," *Mechanics of Time-Dependent Materials*, Vol. 20, No. 1, pp. 1-12, 2016
5. X. Zhao, X. Wang, Z. S. Wu, and Z. G. Zhu, "Fatigue Behavior and Failure Mechanism of Basalt FRP Composites under Long-Term Cyclic Loads," *International Journal of Fatigue*, Vol. 88, pp. 58-67, 2016
6. A. Ince, "A Generalized Mean Stress Correction Model based on Distortional Strain Energy," *International Journal of Fatigue*, Vol. 104, pp. 273-282, 2017
7. D. H. Hwang and S. S. Cho, "Mean Stress Effects in Fretting Fatigue Life Estimation Method using Fatigue Damage Gradient Correction Factor," *Journal of Mechanical Science & Technology*, Vol. 31, No. 9, pp. 4195-4202, 2017
8. D. J. Bang, A. Ince, and L. Q. Tang, "A Modification of UniGrow 2-Parameter Driving Force Model for Short Fatigue Crack Growth," *Fatigue & Fracture of Engineering Materials & Structures*, Vol. 42, pp. 45-60, 2019
9. C. B. Su, Y. Shui, Z. L. Wang, and T. Zafar, "A Time-Dependent Probabilistic Fatigue Analysis Method Considering Stochastic Loadings and Strength Degradation," *Advances in Mechanical Engineering*, Vol. 10, No. 7, pp. 1-9, 2018
10. Z. Q. Fu, Y. X. Wang, B. H. Ji, and T. J. Liu, "Assessment Approach for Multiaxial Fatigue Damage of Deck and U-Rib Weld in Steel Bridge Decks," *Construction and Building Materials*, Vol. 189, pp. 276-285, 2018
11. J. X. Gao and Z. W. An, "A New Probability Model of Residual Strength of Material based on Interference Theory," *International Journal of Fatigue*, Vol. 118, pp. 202-208, 2019
12. Z. H. Yu, W. M. Wang, H. M. Cui, and S. H. Wu, "Static Analysis of the Elastic Teeth of the Spring-Toothed Pickup Device," *Journal of Agricultural Mechanization Research*, Vol. 39, No. 4, pp. 27-31, 2017
13. X. Y. Kang, "Research on Parameter Analysis and Optimization Design of Eccentric Telescopic Rod Conveying Device," Master Dissertation, Inner Mongolia University of Technology, 2018
14. H. Liu, "Numerical Simulation of the Influence of Surface Integrity on Fatigue Properties," Master Dissertation, Huazhong University of Science and Technology, 2014
15. H. B. Lv and W. X. Yao, "Residual Strength Model for Component Fatigue Reliability Estimation," *Acta Aeronautica Sinica*, Vol. 21, No. 1, pp. 74-77, 2000
16. F. J. Zuo, "Research on Fatigue Life Prediction and Reliability Method of Mechanical Structures," Master Dissertation, University of Electronic Science and Technology of China, 2016
17. J. R. Schaff and B. D. Davidson, "Life Prediction Methodology for Composite Structures. Part I- Constant Amplitude and Two-Stress Level Fatigue," *Journal of Composite Materials*, Vol. 31, No. 2, pp. 128-157, 1997